



This is a repository copy of *Fatigue performance of flexible steel fibre reinforced rubberised concrete pavements*.

White Rose Research Online URL for this paper:
<http://eprints.whiterose.ac.uk/147005/>

Version: Accepted Version

Article:

Alsaif, A. orcid.org/0000-0002-3057-0720, Garcia, R. orcid.org/0000-0002-6363-8859, Figueiredo, F.P. et al. (4 more authors) (2019) Fatigue performance of flexible steel fibre reinforced rubberised concrete pavements. *Engineering Structures*, 193. pp. 170-183. ISSN 0141-0296

<https://doi.org/10.1016/j.engstruct.2019.05.040>

Article available under the terms of the CC-BY-NC-ND licence
(<https://creativecommons.org/licenses/by-nc-nd/4.0/>).

Reuse

This article is distributed under the terms of the Creative Commons Attribution-NonCommercial-NoDerivs (CC BY-NC-ND) licence. This licence only allows you to download this work and share it with others as long as you credit the authors, but you can't change the article in any way or use it commercially. More information and the full terms of the licence here: <https://creativecommons.org/licenses/>

Takedown

If you consider content in White Rose Research Online to be in breach of UK law, please notify us by emailing eprints@whiterose.ac.uk including the URL of the record and the reason for the withdrawal request.



eprints@whiterose.ac.uk
<https://eprints.whiterose.ac.uk/>

Fatigue Performance of Flexible Steel Fibre Reinforced Rubberised Concrete Pavements

Abdulaziz Alsaiif^{a,b*}, Reyes Garcia^{a,c}, Fabio P. Figueiredo^a, Kyriacos Neocleous^d,
Andreas Christofe^d, Maurizio Guadagnini^a, Kypros Pilakoutas^a

^aDepartment of Civil and Structural Engineering, The University of Sheffield, Sir Frederick Mappin Building, Mappin Street, Sheffield, S1 3JD, UK.

^bDepartment of Civil Engineering, King Saud University, P. O. Box 800, Riyadh 11421, Saudi Arabia.

^cSchool of Engineering, The University of Warwick, Library Road, Coventry, CV4 7AL, UK.

^dDepartment of Civil Engineering and Geomatics, Cyprus University of Technology, Achilleos 1 Building, Saripolou 2-8, P.O.Box 50329, 3603 Limassol, CY, Cyprus.

Corresponding author: email: asaalsaiif1@sheffield.ac.uk; Tel: +44 (0) 114 222 5729,

Fax: +44 (0) 114 2225700

Abstract

Recycled rubber particles and steel fibres from end-of-life tyres have the potential to enhance the flexibility and ductility of concrete pavements and produce more sustainable pavement solutions. However, the fatigue behaviour of such pavements is not fully understood. This article investigates the mechanical and fatigue performance of steel fibre reinforced concrete (SFRC) and steel fibre reinforced rubberised concrete (SFRRuC). Specimens tested were cast using rubber particles as replacement of natural aggregates (0%, 30% and 60% by volume), and using a blend of manufactured and recycled tyre steel fibres (40 kg/m³). Prisms were subjected to four-point flexural cyclic load ($f=15$ Hz) at stress ratios of 0.5, 0.7, 0.8 and 0.9. The results show that, compared to plain concrete, the addition of steel fibres alone improves the fatigue stress resistance of concrete by 11% (at 25% probability of failure). The replacement of natural aggregates with rubber particles improves the flexibility of SFRRuC (from 51 GPa elastic modules for plain concrete to 13 GPa for SFRRuC), but reduces its fatigue stress resistance by 42% (at 25% probability of failure). However, a probabilistic analysis of the fatigue life data and overall design considerations show that the flexible SFRRuC can be used for pavements. To account for the effect of fatigue load, the Concrete Society approach included in TR34 is modified to account for SFRRuC pavements. Finite element analyses show that flexible SFRRuC pavements can accommodate large subgrade movements and settlements and result in much smaller cracks (up to 24 times) compared to SFRC pavements.

37 **Keywords:** Rubberised concrete; Fatigue performance; Steel fibre reinforced rubberised
38 concrete; Flexible concrete pavement; Recycled fibres

39 **1 Introduction**

40

41 Rigid concrete pavements are widely used in the construction of long-lasting roads as they
42 enable a better distribution of load over the subgrade and require overall smaller structural
43 depth, compared to flexible asphalt pavements. However, road pavement slabs are subjected to
44 continuous cyclic traffic and thermal loads that can deteriorate the material mechanical
45 properties, propagate cracks and eventually cause fatigue fracture [1-3], leading to premature
46 pavement failure. A potential solution to enhance the flexibility, toughness and fatigue
47 resistance of concrete pavements is to replace part of the natural aggregates with waste tyre
48 rubber (WTR) particles [4, 5]. Rubber aggregates are known to reduce stiffness and enhance
49 impact and skid resistance of concrete [6-12], but can cause significant decrease in mechanical
50 properties, especially at high rubber contents (up to 90% reduction in compressive strength for
51 100% natural aggregates replacement) [13-17]. Consequently, until now rubberised concrete
52 (RuC) is mainly utilised in low-strength non-structural applications, e.g. concrete pedestrian
53 blocks [11]. Few researchers studied the performance of RuC in structural applications and to
54 date there are limited studies on the fatigue performance of RuC [7, 18-23]. Liu et al. [7] studied
55 the effect of replacing small percentages of fine natural aggregates with crumb rubber particles
56 (0 to 15% by volume) and found that the fatigue performance of the RuC mixes was better than
57 that of ordinary concrete. The enhancement was attributed to the ability of rubber to resist crack
58 propagation by filling internal spaces and absorbing energy through deformation.

59

60 To enhance the strength of RuC for structural applications (especially flexural strength), steel
61 fibres can be used to produce steel fibre reinforced rubberised concrete (SFRRuC) [5, 20, 24-
62 26]. In SFRRuC, rubber particles absorb energy and enhance the fracture characteristics of the
63 material [14, 27], whereas the fibres control crack opening and propagation even after the peak
64 load, thus dissipating energy through gradual fibre debonding [8]. Ganesan et al. [20] examined
65 the flexural fatigue behaviour of self-compacting RuC (SCRuC) with and without
66 manufactured steel fibres. They observed that the replacement of fine aggregates with crumb
67 rubber particles (up to 20% by volume) improved the flexural fatigue strength by
68 approximately 15%. The addition of crimped-type manufactured steel fibres (MSF) into
69 SCRuC mixes further enhanced the fatigue strength by 10%. More recently, Gupta et al. [22]
70 reported that the incorporation of rubber ash and rubber fibres in concrete as a replacement of
71 fine natural aggregates (up to 35% by volume) enhanced the flexural impact and fatigue
72 resistance by up to 217% and 52%, respectively.

73 Whilst these studies examined the fatigue of mixes with small amounts of rubber (less than
74 20% by total aggregate volume), recent research [8] has proven that the use of large amounts
75 of rubber (especially large rubber particles) is necessary to attain low stiffness pavements with
76 the potential to accommodate subgrade movements. The authors [8] have recently proposed
77 optimised flexible SFRRuC mixes with large amounts of rubber (60% by volume replacement
78 of natural aggregates) and blends of MSF and recycled tyre steel fibres (RTSF) that meet the
79 flexural strengths of EN 13877-1 [28]. The authors [29, 30] also demonstrated that the
80 durability, long-term and permeability performance indicators of the optimised mixes, rank
81 them as ‘highly durable concrete’[31-34]. These properties make SFRRuC a promising
82 candidate for sustainable road pavement slabs, particularly considering that reusing end-of-life
83 tyre materials (WTR and RTSF) in concrete would contribute to the reduction of the
84 environmental impact caused by discarded tyres (1.5 billion units/year [35]). However, to date,
85 the flexural fatigue performance of SFRRuC with large amounts of rubber and steel fibres has
86 not been investigated.

87
88 As the variability in flexural fatigue performance of steel fibre reinforced concrete (SFRC) and
89 SFRRuC is expected to be high due to the combination of rubber and/or fibres [20, 22], a
90 statistical approach may need to be adopted to quantify the reliability of experimental results
91 and their suitability for use in pavement design. Probabilistic distribution models including the
92 two-parameter Weibull distribution model, graphical interpolation model and the mathematical
93 model are commonly used to statistically analyse fatigue life data and derive probabilistic
94 relationships that can be used in design [1, 36, 37].

95
96 This study assesses the mechanical and fatigue performance of SFRRuC. Initially, the study
97 examines the mechanical performance of SFRC and SFRRuC mixes with different replacement
98 volumes of rubber aggregates (0, 30 and 60%) and a blend of MSF and RTSF. The results are
99 compared in terms of uniaxial compressive strength, static flexural strength, elastic modulus,
100 and flexural fatigue strength (number of fatigue cycles). Subsequently, three different
101 probabilistic approaches are used to estimate the fatigue life. The design implications of using
102 SFRRuC in new pavements is shown by a practical example. Finite element analyses are
103 performed using Abaqus® to demonstrate the capability of flexible SFRRuC pavements to
104 accommodate subgrade movements and settlements. This study contributes towards
105 developing economically and structurally sound alternative materials for sustainable flexible
106 concrete pavements, as well as towards using recycled materials derived from end-of-life tyres.

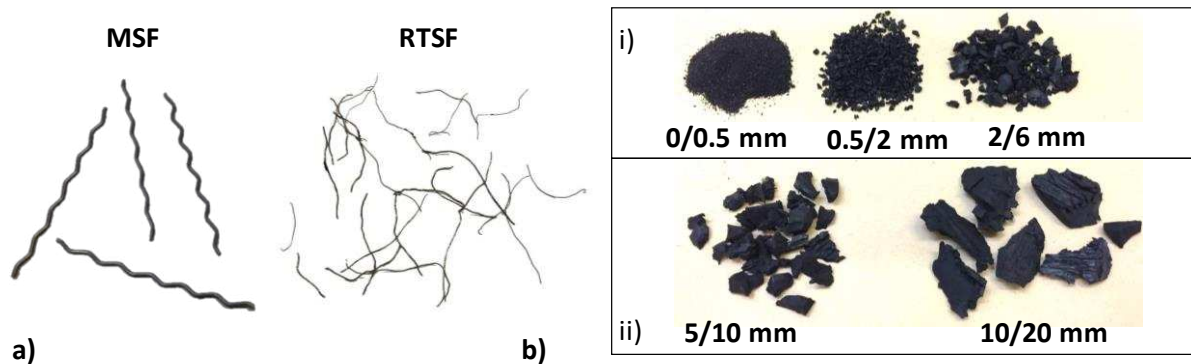
107 **2 Experimental programme**

108

109 **2.1 Materials and casting procedure**

110

111 Four optimised concrete mixes developed previously by the authors [8, 11, 29] were produced
112 to cast the tested specimens. Three cubes (100 mm) and twelve prisms (100×100×500 mm)
113 were cast and prepared for each mix. A binder made of 80% of a Portland limestone cement
114 CEM II-52.5 N, 10% of silica fume (SF) and 10% of pulverised fuel ash (PFA) was used for
115 all concrete mixes. The fine aggregate was medium-grade washed river sand with size 0/5 mm
116 and specific gravity (SG) of 2.65, whereas the coarse aggregate was round river washed gravel
117 with particle sizes of 5/10 mm and 10/20 mm and SG of 2.64. Chemical admixtures including
118 plasticiser and superplasticiser were utilised to enhance workability and cohesion. A blend of
119 20 kg/m³ of MSF (0.8, 55) and 20 kg/m³ of RTSF (0.22, 23), as shown in Figure 1a, were used
120 as reinforcement. Details on the characterisations of the steel fibres are reported in [8, 38].

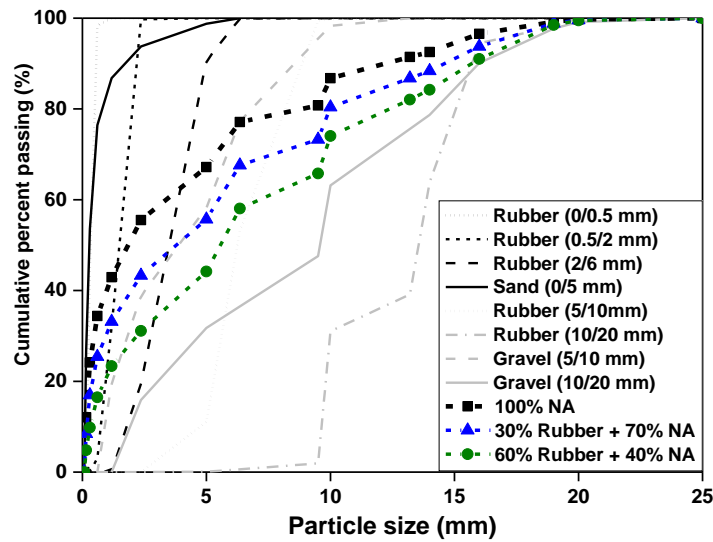


121

122 Figure. 1 a) MSF and RTSF, b) rubber particles, used in this study

123

124 The natural aggregates were replaced with two different volumetric percentages of rubber
125 particles (30% or 60%) of roughly similar size distribution to minimise packing issues. Figure
126 1b shows the rubber particles according to size. The fine rubber particles of sizes 0/0.5 mm,
127 0.5/2 mm and 2/6 mm were used in a 2:3:4 ratio, respectively, whilst the coarse rubber particles
128 of sizes of 5/10 mm and 10/20 mm were used in a 1:1 ratio. The mass of rubber replacing the
129 mineral aggregates was calculated using a relative density of 0.8 [8]. Figure 2 shows the particle
130 size distribution of rubber and natural aggregates (NA) obtained according to ASTM-C136
131 [39].



132

133 Figure. 2 Particle size distributions for rubber particles and natural aggregates

134 Table 1 summarises the mix proportions and corresponding IDs of the four concrete mixes
 135 examined in this study. The number in the ID represents the quantity of rubber particles
 136 replacing both fine and coarse aggregates (0%, 30% or 60% by volume), while P=Plain
 137 concrete and BF=blend fibres.

138 **Table 1.** Mix proportions for 1 m³ of concrete, adapted from [8]

Components	Concrete mixes ID			
	0P	0BF	30BF	60BF
CEM II (kg/m ³)	340	340	340	340
Silica Fume (SF) (kg/m ³)	42.5	42.5	42.5	42.5
Pulverised Fuel Ash (PFA) (kg/m ³)	42.5	42.5	42.5	42.5
Fine aggregates 0/5 mm (kg/m ³)	820	820	574	328
Coarse aggregates 5/10 mm (kg/m ³)	364	364	254	146
Coarse aggregates 10/20 mm (kg/m ³)	637	637	446	255
Water (l/m ³)	150	150	150	150
Plasticiser (l/m ³)	2.5	2.5	3.25	4.25
Superplasticiser (l/m ³)	5.1	5.1	5.1	5.1
Fine rubber particles (kg/m ³)	0	0	165	330
Course rubber particles (kg/m ³)	0	0	24.8	49.6
MSF (kg/m ³)	0	20	20	20
RTSF (kg/m ³)	0	20	20	20
Total	2404	2444	2087	1733

139

140 To produce the SFRRuC mixes, natural and rubber aggregates were first added into a pan mixer
 141 and mixed for approximately 30 s in dry conditions. Half of the mixing water was then added,
 142 and the materials were mixed for 1 min. The mixer was halted for three minutes to add the

143 binder materials. Subsequently, mixing restarted and the remaining water and admixtures were
144 gradually added for another 3 min. Finally, the steel fibres were added manually, and mixing
145 continued for 3 min. All specimens were cast in moulds using two layers of concrete
146 (according to EN 12390-2 [40]), and each layer was compacted on a vibrating table for 25 s.
147 Following casting, the specimens were covered with plastic sheets to retain moisture, and kept
148 under standard laboratory conditions for 2 days. As a large number of specimens were needed
149 for each mix, due to parallel durability studies [29, 30], three batches were cast for each mix.
150 The number of specimens per mix was also limited by the capacity of the concrete mixer in the
151 laboratory. All specimens were cured in a mist room for 28 days, after which they were stored
152 under standard laboratory conditions until testing. All specimens were tested after 150 days
153 following casting to ensure that they had developed their full strength.

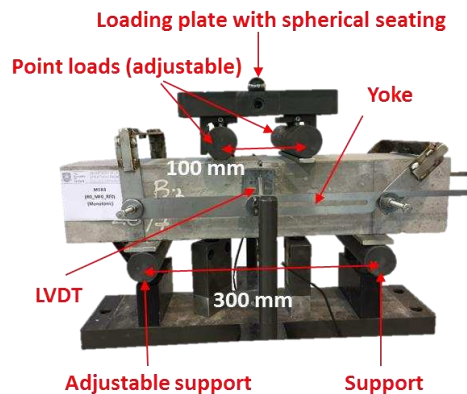
154

155 **2.2 Test setup and instrumentation**

156

157 The uniaxial compressive tests on cubes were carried out using a cube crusher at a loading rate
158 of 0.4 MPa/s, according to EN 12390-3 [41]. The prisms were subjected to static and fatigue
159 four-point bending using a servo-hydraulic actuator with a capacity of 250 kN ($\pm 0.05\%$ error).
160 Two linear variable differential transducers (LVDTs) mounted onto each side of a yoke, as
161 suggested by the JSCE guidelines [42] (see Figure 3), monitored the vertical mid-span
162 displacement of the prisms. The static tests were performed at a displacement rate of 0.2
163 mm/min. Initially, three prisms per mix were tested statically to select the load limits for the
164 fatigue tests and to monitor the development of cracks. The maximum amplitude of the fatigue
165 load was calculated by multiplying a stress ratio ($S=0.5, 0.7$ or 0.9) by the average flexural
166 strength obtained from the three specimens subjected to static load. As discussed in more detail
167 in section 3.3, in some cases the stress ratio was multiplied by the characteristic flexural
168 strength (instead of the average) to prevent premature failure of the prisms during the fatigue
169 tests. The minimum amplitude of each loading cycle was set to 10% of the maximum fatigue
170 load to avoid disengagement of the specimens during testing. The fatigue loading cycles were
171 applied at a frequency of 15 Hz (sinusoidal wave), which is within the typical range (12-20 Hz)
172 used for prism tests in order to avoid amplification or resonance problems [1, 19, 36, 43, 44].
173 The load cycles were applied in four point bending, ensuring a sufficient constant moment
174 region to allow the development of cracked sections at a known stress level. The fatigue tests
175 were terminated either after two million cycles, or at failure of the prisms. Readings were saved
176 at specific logarithmic steps as following (every cycle from 0 to 10 then every 10th cycle up to

177 100 cycles, then every 100th cycle up to 1,000 cycles, then every 1,000th cycle up to 10,000
178 cycles, then every 10,000th cycle up to failure). The main output of the fatigue tests was the
179 number of cycles at failure as well as the vertical displacements recorded by the LVDTs.



180
181

Figure. 3 Flexural test set-up

182 3 Results and discussion

183

184 3.1 Failure mode

185

186 Typical failure modes of the tested cubes are shown in Figure 4. Whilst the plain concrete
187 specimens (OP) failed in a brittle manner, the SFRC and SFRRuC specimens failed in a much
188 more ‘ductile’ manner. As the inclusion of large amounts of rubber and steel fibres led to the
189 development of more distributed (and thinner) cracking, compared to specimens without rubber
190 (0BF), this confirms that ductility was improved by adding fibres and further enhanced by the
191 rubber, as explained previously by the authors in [8].



192
193

Figure. 4 Typical failure modes of concrete cubes

194 3.2 Static compressive and flexural strengths

195

196 Table 2 summarises the average cube compressive strength ($f_{cm,cube}$), static flexural elastic
197 modulus (E_s), and static flexural strength ($f_{ctm,fl}$) including characteristic values ($f_{ctk,fl}$) for each

198 concrete mix. The coefficient of variation is also presented in brackets. The results in Table 2
 199 indicate that the addition of a blend of steel fibres in conventional concrete (mix 0BF) increases
 200 the compressive strength by 18% over the plain concrete mix (0P). A similar enhancement was
 201 observed in a previous study by the authors [8], who attributed the enhancement to the ability
 202 of steel fibres (especially RTSF) to control and delay micro-crack coalescence and the unstable
 203 propagation of cracking. However, mixes 0BF and 0P show the same elastic modulus and
 204 flexural strength despite the difference in compressive strength, which may be attributed to
 205 some air being trapped during the casting of 0BF prisms as observed by the authors in another
 206 study [8]. Indeed, the results in [8] showed that the increase in air content creates weaknesses
 207 inside the concrete matrix and decreases concrete density, which in turn affects both the
 208 strength and stiffness. Compared to mix 0P, replacing large amounts of fine and coarse
 209 aggregates with rubber reduces the compressive strength by 49% and 85% for 30BF and 60BF
 210 mixes, respectively. Similarly, the elastic modulus and flexural strength of mix 30BF drop by
 211 57% and 34%, respectively, whereas these properties decrease by 75% and 42% for mix 60BF.
 212 Nevertheless, in the design of road pavements, which work essentially in bending, having
 213 sufficient flexural strength is more important than having high compressive strength, provided
 214 durability is not compromised.

215 Table 2. Static compressive and flexural test results

Mix	$f_{cm,cube}$ (MPa)	E_s (MPa)	$f_{ctm,fl}$ (MPa)	$f_{ctk,fl}$ (MPa)	$\frac{f_{ctm,fl}}{\sqrt{f_{cm,cube}}}$
0P	102 (4.7)	51 (5.1)	7.0 (13.3)	5.2	0.693
0BF	120 (2.9)	51 (4.8)	7.0 (9.3)	5.8	0.639
30BF	52 (7.5)	22 (13.8)	4.6 (5.3)	4.1	0.638
60BF	15 (10.7)	13 (21.9)	4.1 (18.5)	2.6	1.058

216
 217 The reduction in strength and stiffness in SFRRuC is mainly due to the lower stiffness and
 218 higher Poisson's ratio of rubber (nearly 0.5) when compared to natural aggregates, but also due
 219 to the poor adhesion between rubber and cement paste [8, 11, 15]. It should be noted that the
 220 compressive strength of the mixes degrades faster than the flexural strength, which confirms,
 221 as also discussed in [8], that the combination of fibres and rubber enhances the tensile capacity
 222 of SFRRuC. This is evident by noting that the ratio of the average static flexural strength to the
 223 square root of the average compressive strength ($\frac{f_{ctm,fl}}{\sqrt{f_{cm,cube}}}$) for 60BF is much higher than for
 224 the other mixes.

225 It should be mentioned that the relatively large variability in $f_{ctm,fl}$ in Table 2 can be attributed
 226 to the fact that each specimen belonged to a different batch. To determine a safe initial loading

227 protocol for the fatigue stress loads, the characteristic flexural strength ($f_{ctk,fl}$) of each mix was
 228 determined according to RILEM TC 162-TDF [45].

229

230 3.3 Flexural fatigue strength

231

232 Table 3 summarises the flexural fatigue results of the tested prisms. The results report the stress
 233 ratio (S) in decreasing order, as well as the fatigue life (N). For the initial tests (3 prisms per
 234 mix), the maximum and minimum amplitudes of the fatigue load were determined using the
 235 characteristic strength values ($f_{ctk,fl}$) and $S=0.9$ (see footnote * in Table 3). After examining the
 236 values N at this stress ratio, it was found that some of the plain concrete (OP) and SFRC
 237 specimens (OBF) sustained at least 2 million cycles. Conversely, the N values of the SFRRuC
 238 specimens (30BF and 60BF) were much lower. Hence, it was decided to use average strength
 239 values ($f_{ctm,fl}$) and S of 0.8 and 0.9 for the tests on prisms OP and OBF, respectively. On the
 240 other hand, the flexural fatigue loads for the tests on prisms 30BF and 60BF were determined
 241 using characteristic values and S of 0.7 and 0.5.

242

243

Table 3. Fatigue flexural test results

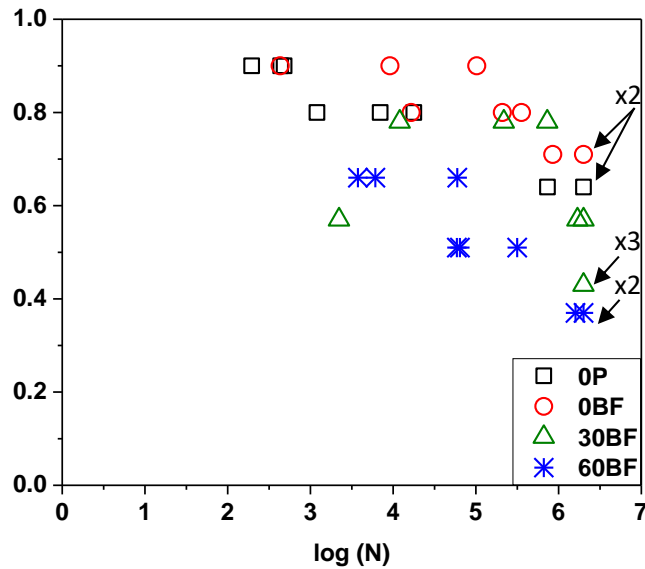
Mix	Stress ratio, S, based on $f_{ctm,fl}$ ($f_{ctk,fl}$)	Specimen No.	Fatigue life, N	Mix	Stress ratio, S, based on $f_{ctm,fl}$ ($f_{ctk,fl}$)	Specimen No.	Fatigue life, N		
OP	0.9 (1.26)	OP-1	195	30BF	0.78 (0.9*)	30BF-1	12,000 ⁺		
		OP-2	438			30BF-2	217,700 ⁺		
		OP-3	482			30BF-3	729,700 ⁺		
	0.8 (1.12)	OP-1	1,200 ⁺		30BF-1	2,218			
		OP-2	6,968		30BF-2	1,690,882			
		OP-3	17,800 ⁺		30BF-3	2,000,000			
	0.64 (0.9*)	OP-1	733,303		30BF-1	2,000,000			
		OP-2	2,000,000		30BF-2	2,000,000			
		OP-3	2,000,000		30BF-3	2,000,000			
	OBF	0.9 (1.13)	OBF-1		431	60BF	0.66 (0.9*)	60BF-1	3,754
			OBF-2		9,172			60BF-2	6,084
			OBF-3		102,718			60BF-3	59,690
0.8 (1.0)		OBF-1	16,525	60BF-1	58,937				
		OBF-2	209,338	60BF-2	64,157				
		OBF-3	356,807	60BF-3	315,080				
0.71 (0.9*)		OBF-1	852,009	60BF-1	1,600,000				
		OBF-2	2,000,000	60BF-2	2,000,000				
		OBF-3	2,000,000	60BF-3	2,000,000				

244 ⁺ Number of cycles recorded in 100 cycle accuracy.

245 * Initial tests at $0.9f_{ctk,fl}$

246

247 Figure 5 compares the logarithmic number of cycles ($\log N$) endured by each specimen and the
 248 relative S calculated using $f_{ctm,fl}$ (quantitative comparisons are included in section 4). It is
 249 evident that the fatigue life data have a large scatter even for the same mixes and stress ratios,
 250 in particular for specimens with steel fibres and/or rubber particles. Though the uneven
 251 distribution of rubber and fibre orientation may significantly contribute to this high variability
 252 [1, 20], the fact that specimens from different batches were used also plays a significant role.



253

254 Figure. 5 Test results in terms of logarithmic number of cycles ($\log N$) and S (based on $f_{ctm,fl}$)

255

256 Figure 5 indicates that steel fibre blends improve the performance of specimens 0BF by
 257 increasing its fatigue life. Previous research has proven that RTSF are effective in restraining
 258 the propagation of micro-cracks into meso-cracks, whilst MSF are more effective in holding
 259 macro-cracks together [1, 38].

260

261 The replacement of natural aggregates with rubber in SFRRuC significantly degrades the
 262 fatigue performance of specimens 30BF and 60BF. This can be attributed to the stiffness and
 263 strength degradation in the SFRRuC resulting from the different elastic properties of rubber,
 264 as well as to the weak bond between cement paste and rubber. SFRRuC is also highly porous
 265 [29], which also contributes to stiffness degradation during cyclic loading.

266

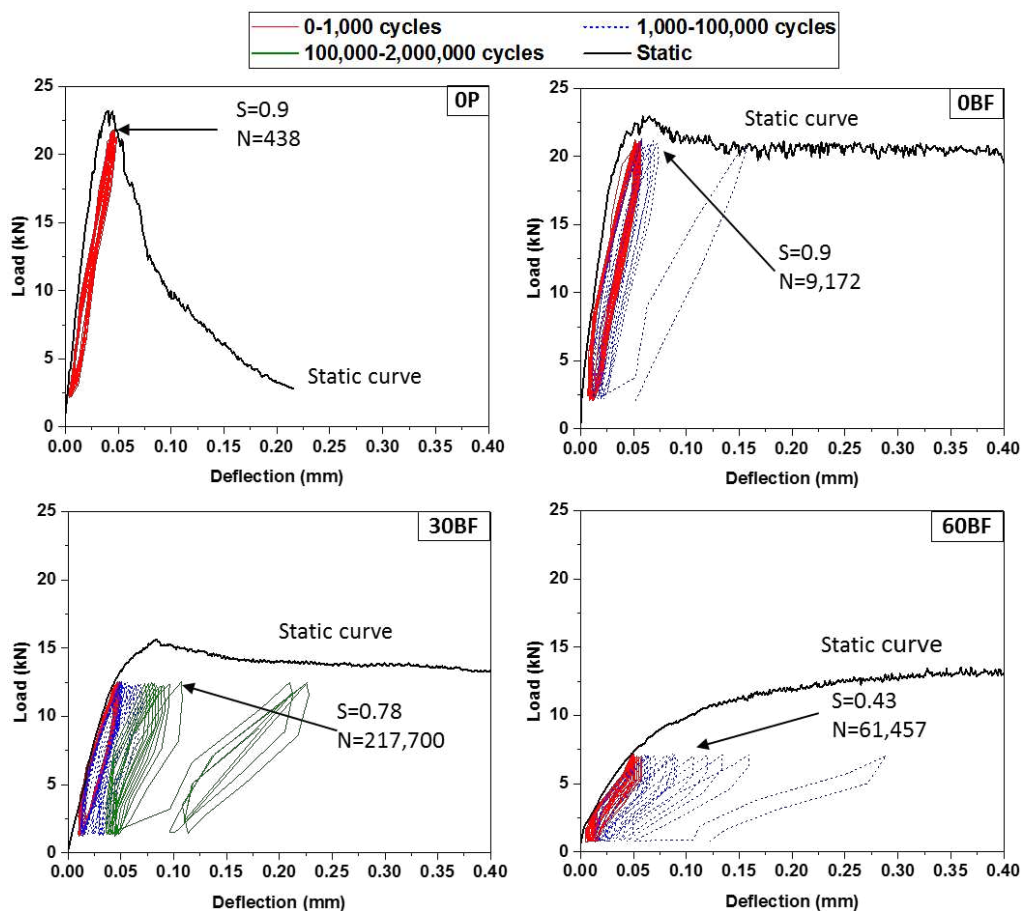
267 Figure 6 compares the load-deflection response under static and fatigue load for the examined
 268 mixes. The static curve is the average of three prisms, whereas the fatigue curve (one specimen)
 269 is representative of typical behaviour observed during the tests. Despite the fact that the applied
 270 S (calculated using $f_{ctm,fl}$) is different for all mixes, it is evident that the initial stiffness (slope)

271 of the fatigue loops is similar to that of the static curve. However, the stiffness degrades
 272 gradually with the number of fatigue cycles. Note also that the stiffness degrades faster with
 273 increasing rubber contents. It is also interesting to note that the OP and OBF failure occurred
 274 when the fatigue cycles touched the monotonic envelope. This may also be the case for 30BF
 275 and 60BF as one cycle was recorded for every logarithmic step. Though this does not
 276 necessarily help to predict fatigue life, but it can give an indication of the likely fatigue
 277 behaviour and, most importantly, the maximum displacement at failure.

278

279 The damage process in SFRRuC under fatigue loading is expected to progress in three stages:
 280 1) during the first load cycles, flaws and micro-cracks form at the rubber/matrix interface and
 281 at the weak region within the concrete; 2) as loading progresses, micro-cracks develop at the
 282 rubber/matrix interface and at the fibre/matrix interface, with the former propagating at a faster
 283 rate. Although the fibres resist the opening of numerous micro-cracks, these tend to propagate
 284 and combine quickly to form macro-cracks; 3) at the final stages of loading (or at failure), a
 285 main crack develops after a sufficient number of macro-cracks have formed.

286



287

288 Figure. 6 Load-deflection response under static and fatigue load for examined mixes

289 The fatigue loops of the SFRRuC (30BF and 60BF) specimens are evidently “fatter” than those
290 of 0P and 0BF, thus indicating that the addition of rubber enhances energy dissipation.
291 However, a direct comparison of the energy dissipated by the specimens is not possible due to
292 the different S applied during the tests. Note also that, due to their higher flexibility, SFRRuC
293 specimens exhibit notably higher deflection at failure than that of normal concrete (0P and
294 0BF). Despite the lower fatigue resistance of SFRRuC mixes with large volumes of rubber,
295 their higher ductility and flexibility can still be used to accommodate subgrade movements of
296 pavement slabs at lower stress levels. To assess the overall fatigue performance of SFRRuC
297 pavement, a probabilistic approach can be adopted, as shown in the following sections.

298

299 **4 Determination of fatigue-life distribution using probabilistic analysis**

300

301 In this section, three models: 1) two-parameter Weibull distribution model, 2) graphical
302 interpolation model and 3) the mathematical model are used to derive probabilities of failure
303 (P_f) and S - N relationships for each mix, which can be used in pavement design. For comparison
304 purposes, the P_f - S - N relationships are compared at probabilities of failure of 25% and 50% (or
305 survival probabilities of 75% and 50%, respectively). These values are widely adopted in the
306 fatigue design of pavements [1, 46-48]. In pavement design, it is usually considered that 2×10^6
307 cycles correspond to an infinite fatigue life [7, 20, 49] and this assumption is utilised in the
308 following calculations.

309

310 **4.1 Two-parameters Weibull distribution**

311

312 The Weibull distribution has been widely used for the statistical analysis of fatigue life data in
313 concrete [7, 36, 49, 50] because it is easy to apply, it is statistically sound and provides accurate
314 results even with a small number of samples, and it has a hazard function that reflects the actual
315 material behaviour in fatigue. The two-parameters of the Weibull distribution (α and u) can be
316 calculated through either i) the graphical method, ii) the method of moments, or iii) the method
317 of maximum-likelihood estimate. In this study, the fatigue life data for each mix and at a given
318 stress ratio S (based on $f_{ctm,i}$) are analysed, and α and u are estimated using methods i to iii
319 above. The mean values of α and u (average of i to iii) are used to estimate the fatigue lives
320 corresponding to $P_f = 0.25$ and 0.50 , from which the P_f - S - N relationships are derived.

321 4.1.1 Graphical method

322

323 The Weibull distribution survival function is defined by [7, 50]:

$$324 P_s(N) = \exp \left[- \left(\frac{N}{u} \right)^\alpha \right] \quad (1)$$

325 where N is the fatigue life, α is the shape parameter (or Weibull slope) at the stress ratio S, and
326 u is the scaling parameter (or characteristic life) at S.

327 By taking the logarithm twice on both sides of Eq. (1):

$$328 \ln \left[\ln \left(\frac{1}{P_s} \right) \right] = \alpha \ln(N) - \alpha \ln(u) \quad (2)$$

329 If it is assumed that $Y = \ln \left[\ln \left(\frac{1}{P_s} \right) \right]$, $X = \ln(N)$ and $\beta = \alpha \ln(u)$, then Eq. (2) can be
330 rewritten as a linear equation:

$$331 Y = \alpha X - \beta \quad (3)$$

332 where all the variables are as defined before. Hence, when the fatigue life data at a given stress
333 follow a linear trend (correlation coefficient $r \geq 0.9$), such data are deemed to comply with the
334 Weibull distribution and α and u can be obtained directly from regression analyses [7, 20].
335 Table 4 summarises the fatigue life data (in ascending order), P_s , X and Y of the tested
336 specimens. In this table, the survival probability P_s is calculated using [49, 50]:

$$337 P_s = 1 - \frac{i}{K + 1} \quad (4)$$

338 where i is the failure order number, and K is the number of specimens tested at a given stress
339 ratio (K=3 prisms).

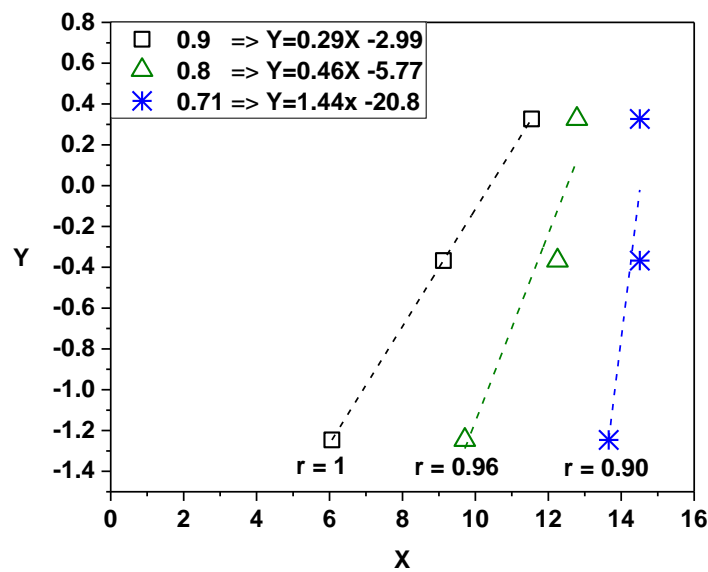
340

Table 4. Analysis of fatigue life data

Mix	S	Fatigue life, N	P _s	X	Y	Graphical method			Method of moments		Maximum likelihood moment		Average		Estimated fatigue life, N _e at P _f of	
						r	α	u	α	u	α	u	α _w	u _w	0.25	0.50
OP	0.9	195	0.75	5.27	-1.25	0.94	1.48	461	2.58	419	3.63	415	2.54	427	262	370
		438	0.50	6.08	-0.37											
		482	0.25	6.18	0.33											
	0.8	1,200	0.75	7.09	-1.25	0.99	0.57	11,208	1.03	8,758	1.13	9,029	0.90	9,569	2,400	6,371
		6,968	0.50	8.85	-0.37											
		17,800	0.25	9.79	0.33											
0.64	733,303	0.75	13.51	-1.25	0.90	1.22	2,032,791	2.29	1,780,997	3.18	1,771,850	2.21	1,843,261	1,048,809	1,561,514	
	2,000,000	0.50	14.51	-0.37												
	2,000,000	0.25	14.51	0.33												
0BF	0.9	431	0.75	6.07	-1.25	1.00	0.29	32,926	0.64	26,868	0.53	22,143	0.48	27,039	2,014	12,594
		9,172	0.50	9.12	-0.37											
		102,718	0.25	11.54	0.33											
	0.8	16,525	0.75	9.71	-1.25	0.96	0.46	272,603	1.15	204,081	1.06	198,163	0.88	222,700	54,233	146,979
		209,338	0.50	12.25	-0.37											
		356,807	0.25	12.78	0.33											
0.71	852,009	0.75	13.66	-1.25	0.90	1.44	2,028,617	2.62	1,820,457	3.74	1,804,209	2.57	1,865,583	1,149,396	1,617,843	
	2,000,000	0.50	14.51	-0.37												
	2,000,000	0.25	14.51	0.33												
30BF	0.78	12,000	0.75	9.39	-1.25	0.99	0.37	396,881	0.86	295,090	0.76	278,790	0.66	320,351	47,821	183,078
		217,700	0.50	12.29	-0.37											
		729,700	0.25	13.50	0.33											
	0.57	2,218	0.75	7.70	-1.25	0.91	0.18	1,999,505	1.16	1,295,849	0.47	818,064	0.60	1,357,428	169,741	736,371
		1,690,882	0.50	14.34	-0.37											
		2,000,000	0.25	14.51	0.33											
0.43	2,000,000	0.75	14.51	-1.25	0.00 ⁺	0.00 ⁺	0.00 ⁺	2,000,000	2,000,000							
	2,000,000	0.50	14.51	-0.37												
	2,000,000	0.25	14.51	0.33												
60BF	0.66	3,754	0.75	8.23	-1.25	0.91	0.49	26,817	0.71	18,660	0.84	20,913	0.67	21,909	3,434	12,701
		6,084	0.50	8.71	-0.37											
		59,690	0.25	11.00	0.33											
	0.51	58,937	0.75	10.98	-1.25	0.85 [*]	0.71	193,571	1.00	145,901	1.29	159,403	0.99	164,629	46,870	113,763
		64,157	0.50	11.07	-0.37											
		315,080	0.25	12.66	0.33											
0.37	1,600,000	0.75	14.29	-1.25	0.90	5.49	2,007,453	9.55	1,965,979	14.25	1,946,702	9.67	1,953,644	1,717,428	1,880,968	
	2,000,000	0.50	14.51	-0.37												
	2,000,000	0.25	14.51	0.33												

⁺ All of three specimens recorded 2M fatigue cycles, therefore, all point in the curve are aligned. ^{*} Correlation coefficient less than 0.9.

343 Figure 7 plots the values X and Y for mix 0BF. The results show that the fatigue life data for
 344 the same stress ratio follow a linear trend. This confirms that α represents the slope of the curve,
 345 while u can be calculated using the curve intercept point. Similar trends were observed for the
 346 rest of the data, and the results of α and u obtained from the graphical method are listed in
 347 Table 4. It is shown that in most cases $r \geq 0.9$, thus indicating that a linear relationship exists
 348 between X and Y. Since all the three prisms 30BF at S=0.43 reached 2×10^6 fatigue cycles, the
 349 three points in the graph are aligned vertically, thus leading to a zero slope (i.e. $\alpha=0$). Although
 350 $r=0.85$ for 60BF at S=0.51, the probabilistic analysis is still carried out and the results are
 351 subsequently adjusted using the average values of the Weibull distribution parameters, as
 352 explained later.



353
 354 Figure. 7 Graphical analysis of fatigue-life data for 0BF
 355

356 4.1.2 Method of moments

357
 358 This method calculates α and u at each stress ratio using the mean (μ) of three prisms, and the
 359 corresponding coefficient of variation (CV) according to the following equations [36, 49-51]:

$$360 \alpha = (CV)^{-1.08} \quad (5)$$

361 and

$$362 u = \frac{\mu}{\Gamma\left(\frac{1}{\alpha} + 1\right)} \quad (6)$$

363 where $\Gamma(\cdot)$ is the gamma function.

364 Table 4 summarises the values α and u for all concrete mixes at various stress ratios using the
365 method of moments.

366

367 **4.1.3 Method of maximum-likelihood estimate**

368

369 The probability density function of the Weibull distribution can be written as [36, 50, 51]:

$$370 \quad f_N(N) = \frac{\alpha}{\theta} N^{\alpha-1} \exp\left[-\frac{N^\alpha}{\theta}\right] \quad (7)$$

371 where

$$372 \quad \theta = u^\alpha \quad (8)$$

373 The maximum-likelihood function can be expressed as follows [36, 50, 51]:

$$374 \quad \frac{\sum_{i=1}^K N_i^{\alpha^*} \ln(N_i)}{\sum_{i=1}^K N_i^{\alpha^*}} - \frac{1}{\alpha^*} = \frac{1}{K} \sum_{i=1}^K \ln(N_i) \quad (9)$$

$$375 \quad \theta^* = \frac{1}{K} \sum_{i=1}^K N_i^{\alpha^*} \quad (10)$$

376 where α^* and θ^* are the maximum-likelihood estimators for α and θ , respectively, and the rest
377 of the variables are as defined before. Accordingly, the value α^* is first obtained iteratively
378 using Eq. (9), and then replaced in Eq. (10) to calculate θ^* . The parameter u is finally calculated
379 using α^* and θ^* (instead of α and θ) in Eq. (8). Table 4 summarises the values α and u for all
380 concrete mixes at various stress ratios using the method of maximum-likelihood estimate.

381

382 The results in Table 4 show that the three methods lead to significantly different values of α
383 and u , with the graphical method yielding α and u values considerably different from those
384 obtained by the other two methods. This is due to the small number of prisms (three) tested at
385 each stress ratio, as well as to the large scatter in the fatigue life data. To address this issue and
386 adopt a more conservative approach, the average values of α and u of the three methods are
387 considered. The average values are shown as α_w and u_w in Table 4.

388

389

390 **4.1.4 Ps-S-N relationships**

391

392 The values α_w and u_w of the Weibull distribution parameters (Table 4) are used here to estimate
 393 the fatigue lives corresponding to $P_f = 0.25$ and 0.50 ($P_s=0.75$ and 0.50). The fatigue life N_e at
 394 certain S and P_f can be estimated using a rearranged version of Eq. (2) [36]:

$$395 \quad N_e = \ln^{-1} \left[\frac{\ln \left[\ln \left(\frac{1}{1 - P_f} \right) \right] + \alpha_w \ln(u_w)}{\alpha_w} \right] \quad (11)$$

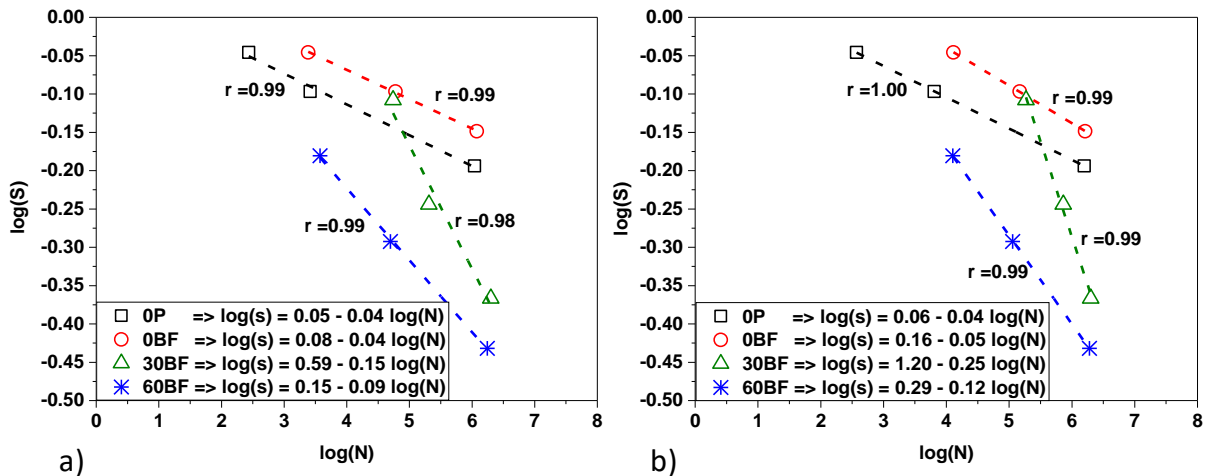
396 Table 4 compares the values N_e calculated using Eq. (11) at $P_f = 0.25$ and 0.50 . The results
 397 show that, as expected, for the same stress ratio the value N_e increases with the probability of
 398 failure. Additionally, for the same probability of failure, N_e increases as the stress ratio
 399 decreases.

400

401 Using the estimated fatigue lives N_e in Table 4, the P_f - S - N relationships can be derived using
 402 the double logarithmic fatigue equation, which has been used in previous studies [7, 19]:

$$403 \quad \log(S) = a + b \log(N_e) \quad (12)$$

404 Figure 8 shows the calculated P_f - S - N relationships for all concrete mixes using N_e values at
 405 $P_f=0.25$ and 0.50 . The constants a and b in Eq. (12) are obtained from regression analyses of
 406 the data shown in Figure 8. It is shown that r is always close to 1 for all concrete mixes at both
 407 probability of failures, which confirms the linear trend of the test data. Note that the equations
 408 in Figure 8 can be used to calculate the stress ratio for a known fatigue life at $P_f=0.25$ and 0.50 ,
 409 as shown in section 4.4.



410

411 Figure. 8 Fatigue curves of all concrete mixes corresponding to a) $P_f = 0.25$ and b) $P_f = 0.50$

412 **4.2 Graphical interpolations**

413

414 The graphical interpolation model is suitable for practical design because it presents concisely
 415 the P_f -S-N relationships, and it is fast and computationally simple. To generate the P_f -S-N
 416 relationships, the specimens are initially sorted in ascending order of fatigue life [44, 52, 53].

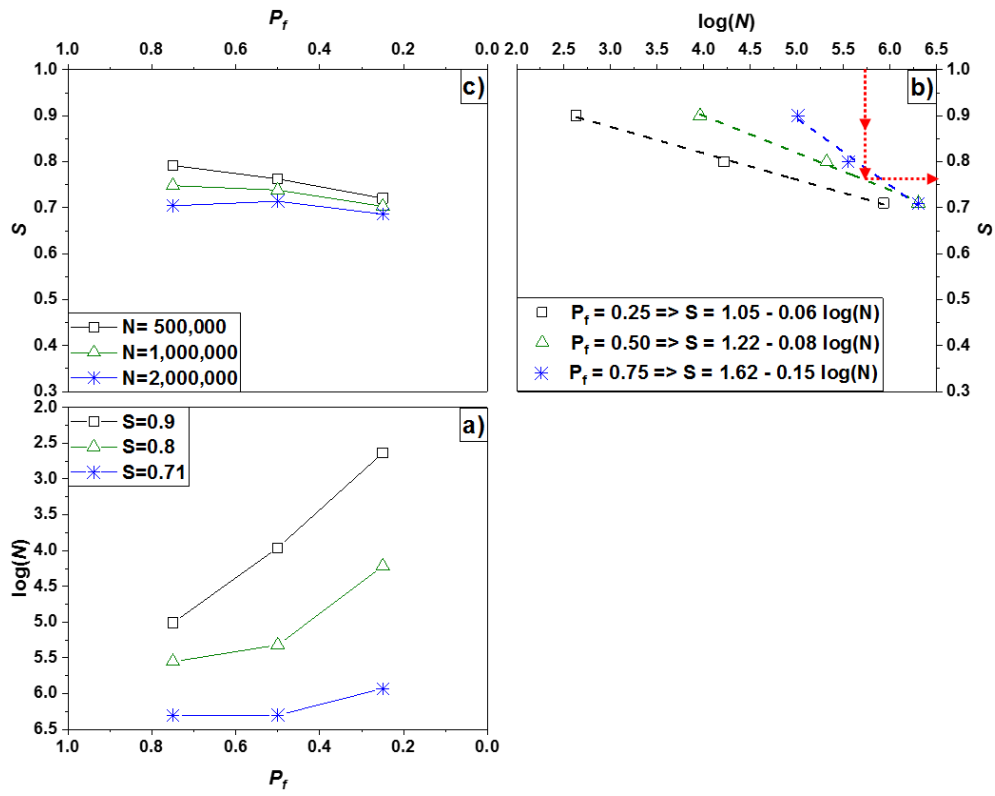
417 The probability of failure is defined as $\frac{j}{n+1}$, where j is the rank of the specimen and n is the
 418 number of specimens tested for each mix at a particular stress ratio. Table 5 shows the
 419 specimens of mix 0BF ranked according to their fatigue life, as well as the calculated P_f values.

420 Table 5. Ranked specimens in terms of N according to stress ratio for mix 0BF.

j	Fatigue life, N, at stress ratio of (based on $f_{ctm,f}$)			$P_f = \frac{j}{(n+1)}$
	0.9	0.8	0.71	
1	431	16,525	852,009	0.25
2	9,172	209,338	2,000,000	0.50
3	102,718	356,807	2,000,000	0.75

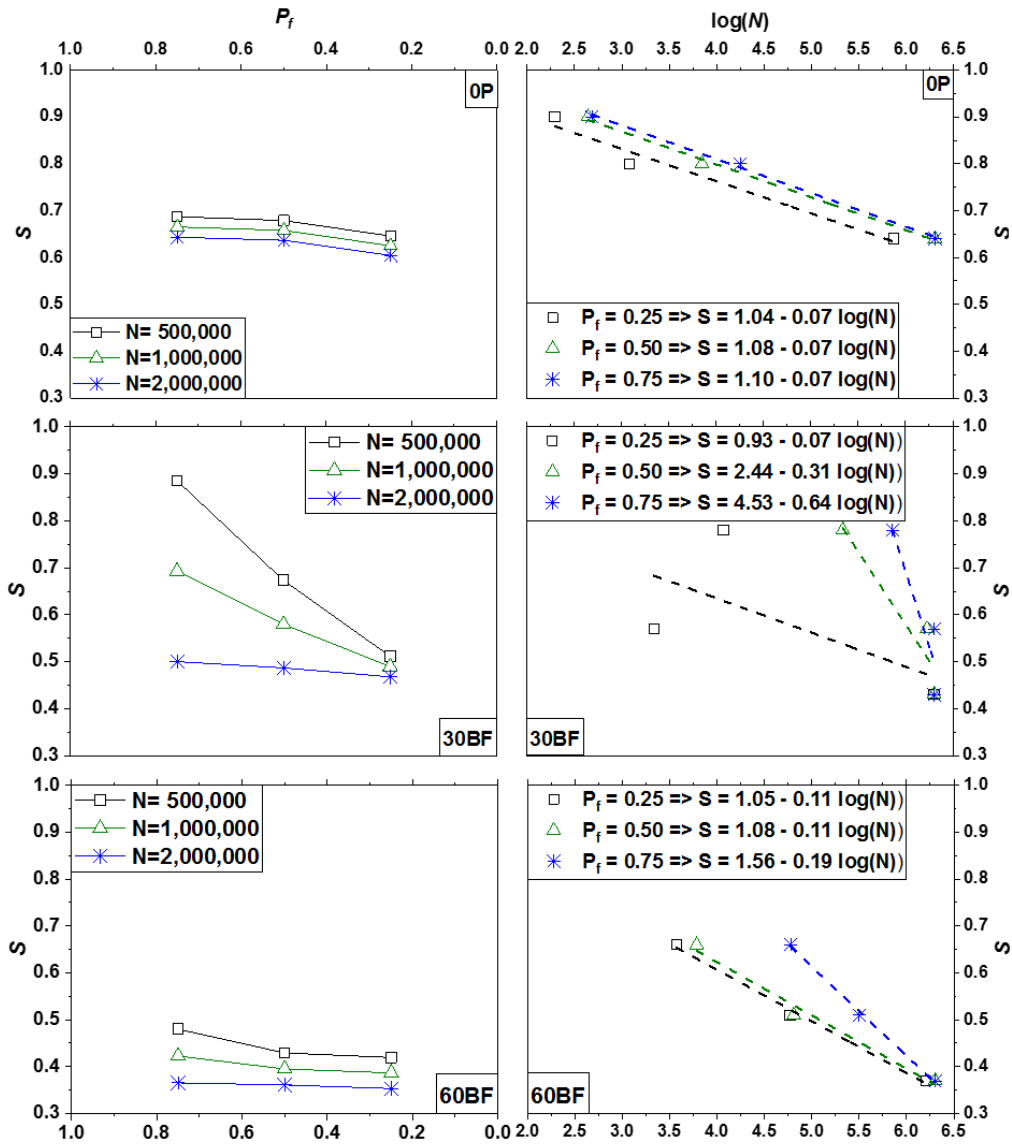
421

422 The P_f -S-N relationships for mix 0BF are shown in Figures 9a-c. In this method, a P_f -N curve
 423 is initially plotted for each stress ratio using P_f and $\log(N)$, as shown in Figure 9a for the data
 424 in Table 5. Based on linear regressions, the S-N curves are then derived using the stress ratios
 425 S (based on $f_{ctm,f}$) and $\log(N)$ for each P_f , as shown in Figure 9b. The S- P_f curves in Figure 9c
 426 are finally obtained by graphical interpolation for different fatigue lives. For instance, for a
 427 fatigue life $N=500,000$ cycles ($\log(N)=5.7$), the estimated stress ratio is $S_e=0.76$ (see Figure
 428 9b) for $P_f=0.50$. Alternatively, the linear equations obtained by regression analyses in the S-N
 429 curves (see Figure 9b) can be used to estimate the stress ratio. Different N can be selected in
 430 the last step for comparison. In this study, $N=500,000$, $1,000,000$ and $2,000,000$ cycles are
 431 adopted. The P_f -S and S-N curves for mixes 0P, 30BF and 60BF calculated following the above
 432 procedure are shown in Figure 10. Further comparisons of the results shown in Figures 9 and
 433 10 are included in section 4.4.



434

435 Figure. 9 Graphical interpolation example for mix 0BF a) P_f - N , b) N - S and c) P_f - S curves



436

437

438 Figure. 10 Graphical interpolation results for mixes OP, 30BF and 60BF: S- P_f and S-N curves

439

440 4.3 Mathematical models

441

442 Previous research has proposed a mathematical function to derive P_f -S-N relationships for
 443 SFRC [1, 44, 52]. The mathematical function can be expressed as:

$$444 P_f = 1 - 10^{-a S^b (\log N)^c} \quad (13)$$

445 where a , b and c are experimental coefficients derived from statistical analyses of the fatigue
 446 life data, as described in references [44, 52, 53]. The coefficient a , b and c obtained for the
 447 mixes examined in this study are summarised in Table 6. Such coefficients can be replaced in
 448 Eq. (13) to estimate the stress ratio S_e for any values of N and P_f .

449 Table 6. Experimental coefficients a, b and c calculated from the mathematical model.

Mix	Experimental coefficients		
	a	b	c
0P	8.77E-04	21.50	8.39
0BF	1.43E-03	10.07	4.76
30BF	2.91E-04	1.71	4.62
60BF	2.27E-06	8.35	10.87

450

451 **4.4 Comparison between models**

452

453 Table 7 compares the estimated fatigue stress ratio S_e for a fatigue life of 2×10^6 cycles and
 454 $P_f=25\%$ and 50% obtained from the probabilistic models described in sections 4.1, 4.2 and 4.3.
 455 With the exception of 30BF, the estimated fatigue stress ratios obtained from the three models
 456 agree well for all mixes at the same P_f . The low stress ratios given by the mathematical model
 457 for 30BF can be attributed to the fact that the three specimens for $S=0.43$ reached 2×10^6 fatigue
 458 cycles (see Table 3), which leads to a very low coefficient b (see Table 6). The average stress
 459 ratio of the three models can be used for practical pavement design, as demonstrated by an
 460 example in the following section.

461 Table 7. Summary of the fatigue stress ratio obtained from three methods.

Mix	P_f	Estimated S_e based on			Average stress ratio, $S_{e,ave}$
		Weibull distribution	Graphical interpolation	Mathematical	
0P	25%	0.62	0.60	0.61	0.61
	50%	0.63	0.64	0.64	0.64
0BF	25%	0.70	0.69	0.65	0.68
	50%	0.70	0.71	0.71	0.71
30BF	25%	0.42	0.47	0.24	0.45 ⁺
	50%	0.44	0.49	0.40	0.47 ⁺
60BF	25%	0.36	0.35	0.34	0.35
	50%	0.37	0.36	0.37	0.37

462 ⁺ Value calculated based on the Weibull distribution and graphical methods only.

463

464 **5 Design implications**

465

466 To assess the effect of the addition of steel fibres and/or rubber on the thickness h of rigid
 467 pavement slabs, a road section with a standard axle load W is assumed. According to

468 Westergaard's empirical-theoretical model [54], the rigid pavement can be modelled as a thin
 469 elastic plate on a soil subgrade. The stress at the edge (critical location) is:

$$470 \quad \sigma_{max} = \frac{0.572 W}{h^2} \left[4 \log \left(\frac{I}{\sqrt{1.6 Z^2 + h^2} - 0.675 h} \right) + 0.359 \right] \quad (14)$$

471 where σ_{max} is the maximum tensile stress of the slab modified to account for fatigue by
 472 multiplying the flexural strength ($f_{ctm,fl}$ listed in Table 2) by the average fatigue stress ratio
 473 $S_{e,ave}$ at $P_f=25\%$ (i.e. values from last column in Table 7); Z is an equivalent contact radius of
 474 the tyre; and I is the radius of the relative stiffness of the slab, defined by:

$$475 \quad I = \sqrt[4]{\frac{E_s h^3}{12 (1 - \nu^2) M_k}} \quad (15)$$

476 where ν is the Poisson's ratio of the slab material; M_k is the modulus of elastic subgrade
 477 reaction; and E_s is shown in Table 2. In this study, M_k is the modulus of resilience of the soil
 478 and measures the ability of the ground to resist immediate elastic deformation under load.

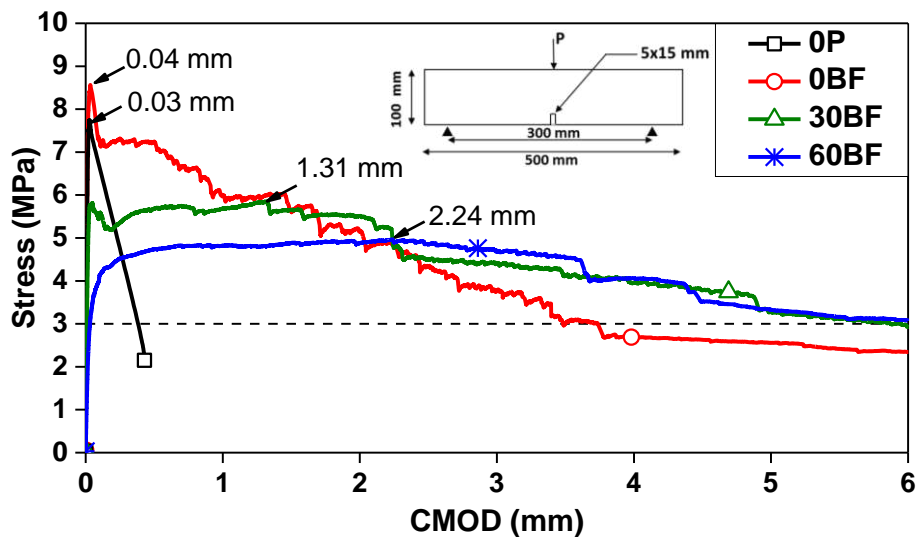
479

480 The slab thickness h for all concrete mixes was calculated using the modified Westergaard's
 481 method and the following (typical) values: $W=80$ kN, $M_k=80$ MPa/m, and $Z=190$ mm
 482 (assuming a tyre pressure of 7 bar), and $\nu=0.2$. The subgrade is taken to be a very well
 483 consolidated made of gravels and sandy gravels [55]. Although mixes 0P and 0BF have similar
 484 average static flexural strength and elastic modulus, the addition of fibres reduces the slab
 485 thickness by 7% ($h=173$ mm for 0P vs $h=161$ mm for 0BF). This is mainly due to the enhanced
 486 fatigue performance resulting from the addition of fibres, as discussed in section 3.3. On the
 487 other hand, the replacement of natural aggregates with rubber particles increases the slab
 488 thickness to 256 mm and 305 mm for mixes 30BF and 60BF, respectively. This is due to the
 489 reduced mechanical and fatigue properties of SFRRuC mixes (sections 3.2 and 3.3), which
 490 leads to a low radius of relative stiffness I (Eq. (15)).

491

492 Based on these results, it is evident that the modified Westergaard's method does not show the
 493 expected benefits of using steel fibres and/or rubber over plain concrete. This is because the
 494 method was originally developed for plain concrete, which behaves in a linear elastic manner
 495 up to tensile failure. As such, the effect of deformability (i.e. ductility and flexibility) which
 496 will help to accommodate subgrade movements are not accounted for in the equations. To
 497 assess the deformability of SFRRuC, the authors performed three-point bending tests on

498 notched prisms according to RILEM [45], and the stress versus crack mouth opening
 499 displacement (CMOD) curves are shown in Figure 11. The enhancement in flexibility is
 500 demonstrated by progressively larger CMODs at maximum stress with increasing rubber
 501 content, resulting from the ability of rubber to reduce stress concentration at the crack tip and
 502 to delay micro-crack propagation [24]. Likewise, the post-peak behaviour is also improved by
 503 the inclusion of fibres, and it is further enhanced by the rubber. For example, at a stress level
 504 of 3MPa, mixes 30BF and 60BF have larger CMODs than that of 0BF, thus confirming the
 505 enhancement in ductility as discussed in section 3.1. Hence, in order to identify the benefits of
 506 using steel fibres and/or rubber in concrete, it is necessary to use design equations that take
 507 into account the flexibility and ductility that SFRRuC can offer.



508
509 Figure. 11 Average stress-CMOD curves for prisms

510
511 The Technical Report 34 (TR34) by the Concrete Society [56] can be used to show the
 512 advantages of using SFRRuC pavements. TR34 designs SFRC slabs at the ultimate limit state
 513 (ULS) using the yield line theory. Accordingly, the flexural moment at the bottom of the slab
 514 and along the sagging yield lines (M_p) are considered to be fully plastic (i.e. residual post-
 515 cracking behaviour exist), as shown in Eq. (16). At the same time, cracks must be avoided at
 516 the top surface of the slab and the moment capacity along the hogging yield lines (M_n), as
 517 shown in Eq. (17), should be always greater than the ultimate design moment of the concrete.

518
$$M_p = \frac{h^2}{1.5} (0.29 \sigma_4 + 0.16 \sigma_1) \quad (16)$$

519
$$M_n = \frac{f_{ctm,fl}}{1.5} \left(\frac{h^2}{6} \right) \quad (17)$$

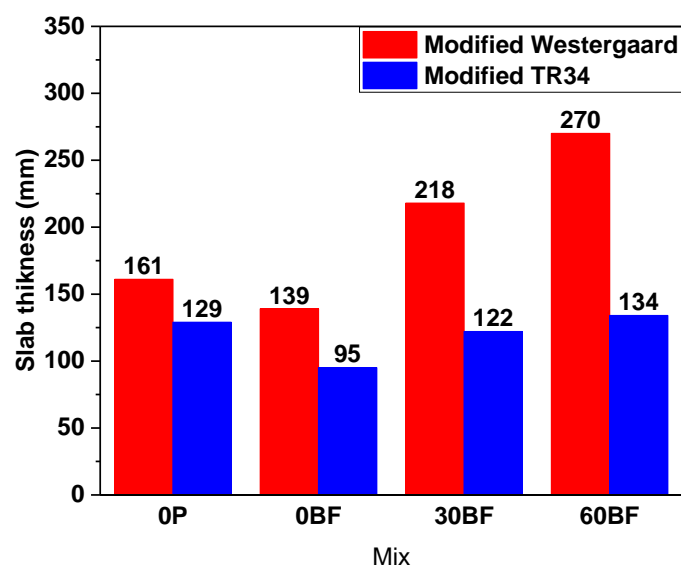
520 where $\sigma_1 = 0.45 \cdot \text{CMOD}_1$, and $\sigma_4 = 0.37 \cdot \text{CMOD}_4$. In this study, values of $\text{CMOD}_1 = 0.5$ mm
 521 and $\text{CMOD}_4 = 3.5$ mm (as obtained from three-point bending tests on notched prisms [45]) are
 522 used to calculate σ_1 and σ_4 . The slab thickness h can be calculated using Eq. (18) [56] for a
 523 free edge load.

$$524 \quad W = \frac{[\pi (M_p + M_n) + 4 M_n]}{[1 - (\frac{2Z}{3I})]} \quad (18)$$

525 The design approach adopted by TR34 neglects the effect of fatigue load. To address this
 526 drawback and account for fatigue, it is thus proposed to modify this approach and multiply
 527 $f_{\text{ctm,fl}}$ in Eq. (17) by $S_{e,\text{ave}}$ (section 4.4).

528

529 Figure 12 compares the slab thickness calculated using the modified TR34 approach and
 530 modified Westergaard's method. It is shown that the adoption of the proposed modified TR34
 531 approach reduces the slab thickness calculated by the modified Westergaard's method by 20%
 532 for OP, 32% for OBF, 44% for 30BF and 50% 60BF mixes. These results confirm the benefits
 533 of using steel fibres and/or rubber in concrete. It is also shown that, although the fatigue
 534 strength of SFRRuC is relatively low, the thickness of slabs produced with this novel material
 535 is similar to that of slabs built with plain concrete. However, unlike plain concrete pavements,
 536 SFRRuC pavements represent a potential solution to accommodate subgrade movements
 537 during service life. Consequently, it is recommended to use the proposed modified TR34
 538 approach for the design of flexible SFRRuC pavements.



539

540

Figure. 12 Slab thickness comparison for all concrete mixes

541 The capability of flexible SFRRuC pavements to accommodate subgrade settlements is
542 demonstrated through finite element (FE) analysis in the following section.

543

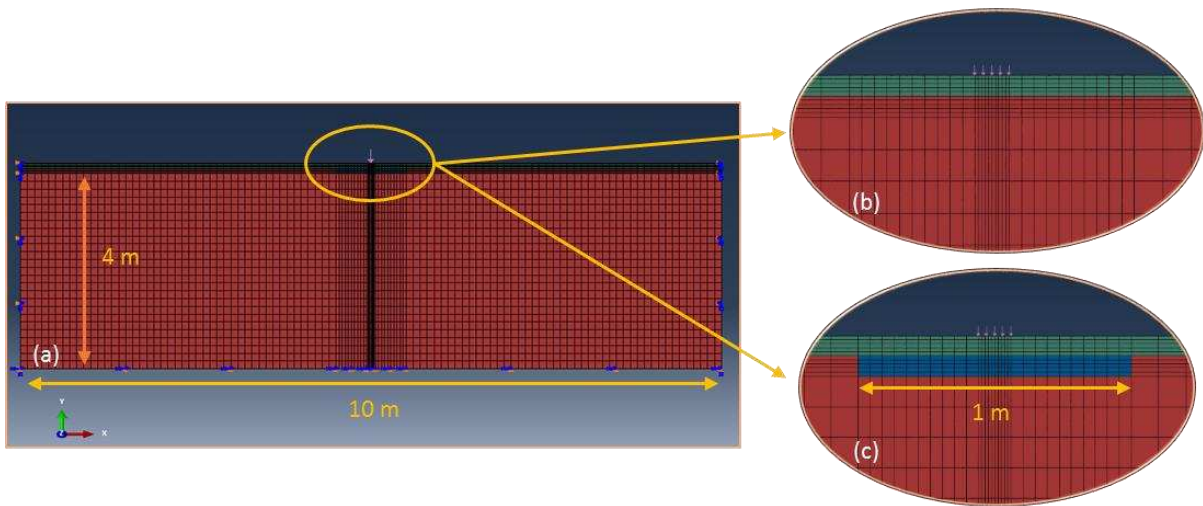
544 **6 Finite Element Modelling**

545

546 A two-dimensional (2D) plane strain model of a pavement slab was developed in the FE
547 software ABAQUS® [57]. Recent research [58] has shown that 2D plane strain models provide
548 similar results to 3D models (differences of less than 2%) in the study of transverse profiles of
549 pavements with large longitudinal dimensions. To show the true benefits of flexible SFRRuC,
550 two pavements designed using the modified TR34 approach (Figure 12) were modelled: i) a
551 SFRC pavement (0BF) of 95 mm depth; ii) a SFRRuC pavement (60BF) of 134 mm depth.
552 The pavements were assumed to be on top of a stiff clay subgrade of length=10.0 m and
553 depth=4.0 m, as shown in Figure 13a. The length of the pavement was chosen to prevent
554 boundary and edge effects. Previous research has shown that there are no subgrade
555 deformations beyond such depth [59]. Two scenarios were considered: 1) a continuous
556 subgrade (Figure 13b), and 2) a subgrade with a gap filled with loose material (length=1 m,
557 depth=0.10 m, see Figure 13c). The gap is intended to simulate common defects arising from
558 non-uniform subgrades due to deterioration developing over time, such as settlement due to
559 poor compaction during construction or temperature variations and freeze-thaw.

560

561 8-node quadrilateral plane strain reduced integration elements (CPE8R) were used for the
562 analyses. An initial convergence analysis was performed to optimise the characteristics of the
563 mesh. Based on these results, only a fine mesh was selected for the loading area. The total
564 number of nodes and elements was 14962 and 4800, respectively.



565
 566 Figure. 13 Finite element model: a) discretised pavement and subgrade, b) continuous
 567 subgrade, c) subgrade with a gap
 568

569 The bottom edge of the subgrade was fixed to prevent horizontal and vertical movements. The
 570 boundary nodes along the pavement edges were constrained horizontally only. A Coulomb
 571 friction law was used to define the surface-to-surface contact interaction between the pavement
 572 and subgrade (friction parameter=0.3). The load (standard axle) on the pavement was applied
 573 through a static contact pressure of 800 kPa. Previous research has widely adopted the Mohr-
 574 Coulomb plasticity criterion for subgrade analysis [60], hence, this criterion is used to model
 575 the inelastic behaviour of the subgrade and the filling material in the gap. Table 8 summarises
 576 the soil properties used in the FE analyses.

577 Table 8. Assumed soil properties used in FE analyses.

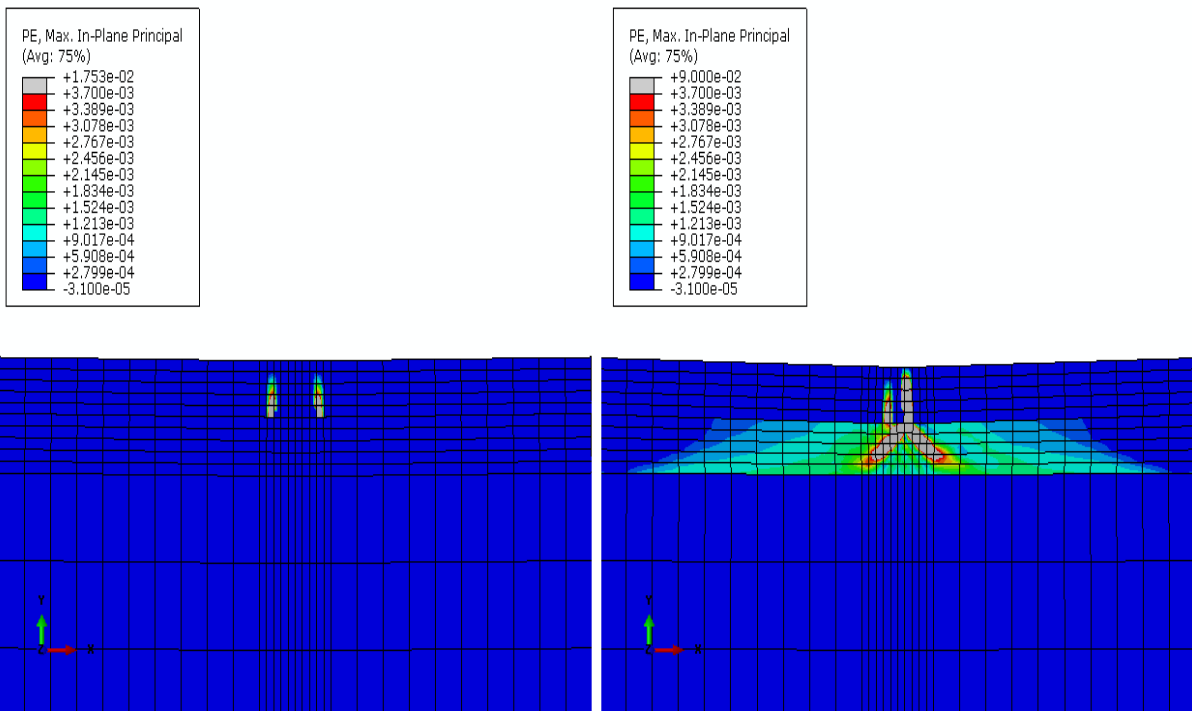
Soil	Elastic modulus (MPa)	Poisson's ratio, ν	Friction angle, ϕ ($^{\circ}$)	Dilation angle ψ ($^{\circ}$)	Yield stress (KPa)	Plastic strain
Stiff Clay (subgrade)	80	0.45	0	0	200	0
Loose Sand (hole filling)	10	0.20	28	0	1	0

578
 579 The concrete was modelled using the concrete damaged plasticity (CDP) constitutive model
 580 built-in in ABAQUS®. This model accounts for the inelastic behaviour of concrete in both
 581 tension and compression, and can include damage. The model considers two main failure
 582 mechanisms in concrete: tensile cracking and compressive crushing. The stress-strain
 583 relationship for uniaxial concrete in tension was obtained using inverse analysis [61, 62]) on

584 the load-deflection curves presented in Figure 6b and d. The values for the CDP model (dilation
 585 angle=30, eccentricity=0.1, $\frac{F_{b0}}{f_{co}} = 1.116$, $K=0.667$ and viscosity= 1×10^{-5}) were taken from
 586 previous research [61, 63, 64] using SFRC.

587

588 Figure 14 compares the plastic strain distribution (cracks) for the SFRC pavement (0BF)
 589 considering the two scenarios. Whilst wide localised cracks develop in both scenarios, the
 590 results in Figure 14b indicate that cracks can be up to 5 times wider if a gap develops under the
 591 pavement. It is also shown that if the pavement settles, two wide cracks propagate through the
 592 pavement towards its top surface within the loaded area. This implies that the pavement would
 593 experience significant damage due to multiple wide cracks, thus jeopardising its serviceability
 594 requirements.

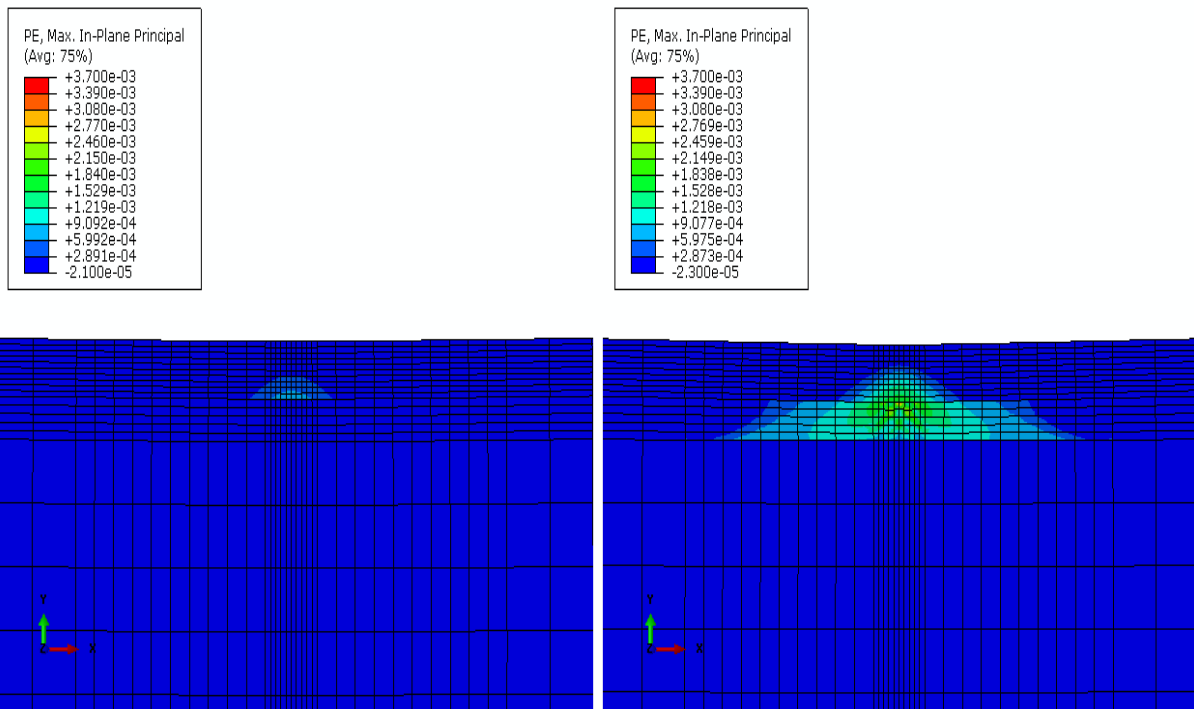


595

596 Figure. 14 Plastic strain model 0BF-95 mm a) without a gap, and b) with 10 cm x 1 m gap.

597 Figure 15 compares the plastic strain distribution (cracks) for the SFRRuC pavement (60BF)
 598 considering both scenarios. Figure 15a shows that some minor cracks develop in the pavement
 599 on the continuous subgrade. However, these cracks are more spread and up to 7 times narrower
 600 compared to the SFRC pavement (see Figure 14a). In presence of the gap (Figure 15b), the
 601 cracks in the SFRRuC pavement are not only more evenly distributed over a larger area, but
 602 also significantly narrower (up to 24 times) than those in the SFRC pavement. Even when the
 603 same depth of 134 mm is used for the SFRC pavement, the cracks are still 10 times larger than

604 the SFRRuC pavement. This shows that flexible SFRRuC pavements are capable of
605 accommodating subgrade movements and settlements more effectively than their SFRC
606 counterparts.



607
608 Figure. 15 Plastic strain for model 60BF-134 mm a) without a gap, and b) with 10 cm × 1 m
609 gap.

610 It should be mentioned that previous research by the authors showed that optimised flexible
611 SFRRuC a) is highly ductile and flexible [8], and b) that such concrete meets the flexural
612 strengths specifications defined in pavement design [28]. The authors have also demonstrated
613 the adequate durability and long term performance of SFRRuC [29, 30]. In this article, the
614 authors prove that (despite its lower fatigue resistance) SFRRuC can accommodate large
615 subgrade movements and settlements. The experimental, analytical and numerical evidence
616 confirm that SFRRuC is a promising solution for building sustainable road pavements,
617 particularly considering that reusing end-of-life tyre materials (WTR and RTSF) in concrete
618 can contribute to reducing stockpiles of discarded tyres. It should be also noted that, due to the
619 limited number of specimens and mixes examined in the above studies, further research is
620 necessary to fully understand the mechanical behaviour and long-term performance of different
621 SFRRuC mixes with other mix proportions and tested with different stress ratios (e.g. 6
622 specimens tested at each stress level). Current research by the authors is validating the
623 predictions given by the modified TR34 approach against additional experiments so as to
624 provide practical design guidelines.

625 **7 Conclusions**

626

627 This study assesses the mechanical and fatigue performance of steel fibre reinforced
628 rubberised concrete (SFRRuC) using fatigue flexural loads on prisms. Based on the results
629 in this study, the following conclusions are drawn:

630

631 • A blend of steel fibres in concrete enhances its compressive strength by 20%, while the
632 flexural strength and elastic modulus remain roughly the same. The addition of rubber as
633 aggregate decreases significantly the compressive strength, static flexural strength and
634 elastic modulus of SFRRuC. However, the combination of fibres and rubber enhances the
635 tensile capacity of SFRRuC.

636

637 • The relationships between probability of failure, stress ratio and fatigue life (P_f - S - N)
638 given by three probabilistic models widely used in pavement design agree reasonably well.
639 They also provide comparable estimates of fatigue stress ratios that can be used for the
640 practical design of SFRRuC pavements.

641

642 • The modified Westergaard's approach does not show the benefits of adding blends of steel
643 fibres or rubber to concrete since the post-peak behaviour of concrete is neglected. The use
644 of the modified TR34 design approach proposed in this study leads to thinner slab thickness
645 when compared to the modified Westergaard's model. Consequently, it is recommended to
646 use this approach for the design of SFRRuC flexible pavements.

647

648 • FE analyses indicate that flexible SFRRuC pavements can accommodate large subgrade
649 settlements, thus making such pavements an attractive solution for road pavement
650 applications.

651

652 **Acknowledgements**

653

654 The authors would also like to thank all of the material suppliers and companies for their in-kind
655 contribution of materials for this research study: Tarmac UK, Sika, Aggregate Industries UK Ltd,
656 Twintech, and Twincon Ltd.

657

658 **Disclosure**

659

660 **Funding:** This study was funded by the European Union Seventh Framework Programme
661 [FP7/2007–2013] under grant agreement no 603722.

662

663

664

665

666

667

668

669

670

671

672

References

- 675 [1] A.G. Graeff, K. Pilakoutas, K. Neocleous, and M.V.N. Peres, *Fatigue resistance and cracking*
676 *mechanism of concrete pavements reinforced with recycled steel fibres recovered from post-*
677 *consumer tyres*, *Engineering Structures* 45 (2012) 385-395.
- 678 [2] P.C. Perdikaris, A.M. Calomino, and A. Chudnovsky, *Effect of fatigue on fracture toughness of*
679 *concrete*, *Journal of engineering mechanics* 112 (8) (1986) 776-791.
- 680 [3] M. Lee and B. Barr, *An overview of the fatigue behaviour of plain and fibre reinforced concrete*,
681 *Cement and Concrete Composites* 26 (4) (2004) 299-305.
- 682 [4] O.A. Abaza and Z.S. Hussein, *Flexural Behavior of Steel Fiber-Reinforced Rubberized Concrete*,
683 *Journal Of Materials In Civil Engineering* 28 (1) (2015) 04015076.
- 684 [5] T. Nguyen, A. Toumi, and A. Turatsinze, *Mechanical properties of steel fibre reinforced and*
685 *rubberised cement-based mortars*, *Materials & Design* 31 (1) (2010) 641-647.
- 686 [6] A. Grinys, H. Sivilevičius, D. Pupeikis, and E. Ivanauskas, *Fracture of concrete containing crumb*
687 *rubber*, *Journal of Civil Engineering and Management* 19 (3) (2013) 447-455.
- 688 [7] F. Liu, W. Zheng, L. Li, W. Feng, and G. Ning, *Mechanical and fatigue performance of rubber*
689 *concrete*, *Construction and Building Materials* 47 (2013) 711-719.
- 690 [8] A. Alsaif, L. Koutas, S.A. Bernal, M. Guadagnini, and K. Pilakoutas, *Mechanical performance of*
691 *steel fibre reinforced rubberised concrete for flexible concrete pavements*, *Construction and*
692 *Building Materials* 172 (2018) 533-543.
- 693 [9] S. Raffoul, R. Garcia, D. Escolano-Margarit, M. Guadagnini, I. Hajirasouliha, and K. Pilakoutas,
694 *Behaviour of unconfined and FRP-confined rubberised concrete in axial compression*,
695 *Construction and Building Materials* 147 (2017) 388-397.
- 696 [10] F. Hernández-Olivares, G. Barluenga, M. Bollati, and B. Witoszek, *Static and dynamic*
697 *behaviour of recycled tyre rubber-filled concrete*, *Cement And Concrete Research* 32 (10)
698 (2002) 1587-1596.
- 699 [11] S. Raffoul, R. Garcia, K. Pilakoutas, M. Guadagnini, and N.F. Medina, *Optimisation of*
700 *rubberised concrete with high rubber content: An experimental investigation*, *Construction*
701 *and Building Materials* 124 (2016) 391-404.
- 702 [12] R. Siddique and T.R. Naik, *Properties of concrete containing scrap-tire rubber—an overview*,
703 *Waste management* 24 (6) (2004) 563-569.
- 704 [13] Z. Khatib and F. Bayomy, *Rubberized portland cement concrete*, *Journal Of Materials In Civil*
705 *Engineering* 11 (3) (1999) 206-213.
- 706 [14] A. El-Dieb, M. Abd El-Wahab, and M. Abdel-Hameed, *Mechanical, Fracture, and*
707 *Microstructural Investigations of Rubber Concrete*, *Journal Of Materials In Civil Engineering*
708 (10) (2008) 640-649.
- 709 [15] A.R. Khaloo, M. Dehestani, and P. Rahmatabadi, *Mechanical properties of concrete containing*
710 *a high volume of tire–rubber particles*, *Waste management* 28 (12) (2008) 2472-2482.
- 711 [16] E. Ganjian, M. Khorami, and A.A. Maghsoudi, *Scrap-tyre-rubber replacement for aggregate*
712 *and filler in concrete*, *Construction and Building Materials* 23 (5) (2009) 1828-1836.
- 713 [17] M.A. Aiello and F. Leuzzi, *Waste tyre rubberized concrete: properties at fresh and hardened*
714 *state*, *Waste Manag* 30 (8-9) (2010) 1696-704.
- 715 [18] C. Wang, Y. Zhang, and A. Ma, *Investigation into the fatigue damage process of rubberized*
716 *concrete and plain concrete by AE analysis*, *Journal Of Materials In Civil Engineering* 23 (7)
717 (2010) 953-960.
- 718 [19] F. Liu, L.-y. Meng, G.-F. Ning, and L.-J. Li, *Fatigue performance of rubber-modified recycled*
719 *aggregate concrete (RRAC) for pavement*, *Construction and Building Materials* 95 (2015) 207-
720 217.
- 721 [20] N. Ganesan, J.B. Raj, and A. Shashikala, *Flexural fatigue behavior of self compacting rubberized*
722 *concrete*, *Construction and Building Materials* 44 (2013) 7-14.

- 723 [21] F. Hernández-Olivares, G. Barluenga, B. Parga-Landa, M. Bollati, and B. Witoszek, *Fatigue*
724 *behaviour of recycled tyre rubber-filled concrete and its implications in the design of rigid*
725 *pavements*, Construction and Building Materials 21 (10) (2007) 1918-1927.
- 726 [22] T. Gupta, A. Tiwari, S. Siddique, R.K. Sharma, and S. Chaudhary, *Response Assessment under*
727 *Dynamic Loading and Microstructural Investigations of Rubberized Concrete*, Journal Of
728 Materials In Civil Engineering 29 (8) (2017) 04017062.
- 729 [23] I. Mohammadi, H. Khabbaz, and K. Vessalas, *In-depth assessment of Crumb Rubber Concrete*
730 *(CRC) prepared by water-soaking treatment method for rigid pavements*, Construction and
731 Building Materials 71 (2014) 456-471.
- 732 [24] A. Turatsinze, J.L. Granju, and S. Bonnet, *Positive synergy between steel-fibres and rubber*
733 *aggregates: Effect on the resistance of cement-based mortars to shrinkage cracking*, Cement
734 And Concrete Research 36 (9) (2006) 1692-1697.
- 735 [25] J.-h. Xie, Y.-c. Guo, L.-s. Liu, and Z.-h. Xie, *Compressive and flexural behaviours of a new steel-*
736 *fibre-reinforced recycled aggregate concrete with crumb rubber*, Construction and Building
737 Materials 79 (2015) 263-272.
- 738 [26] N.F. Medina, D.F. Medina, F. Hernández-Olivares, and M. Navacerrada, *Mechanical and*
739 *thermal properties of concrete incorporating rubber and fibres from tyre recycling*,
740 Construction and Building Materials 144 (2017) 563-573.
- 741 [27] A. Turatsinze, S. Bonnet, and J.-L. Granju, *Mechanical characterisation of cement-based*
742 *mortar incorporating rubber aggregates from recycled worn tyres*, Building and environment
743 40 (2) (2005) 221-226.
- 744 [28] BSI, *EN 13877-1. Concrete pavements Part 1: Materials. BSI 389 Chiswick High Road London*
745 *W4 4AL UK*, (2013).
- 746 [29] A. Alsaif, S.A. Bernal, M. Guadagnini, and K. Pilakoutas, *Durability of steel fibre reinforced*
747 *rubberised concrete exposed to chlorides*, Construction and Building Materials 188 (2018) 130-
748 142.
- 749 [30] A. Alsaif, S.A. Bernal, M. Guadagnini, and K. Pilakoutas, *Freeze-thaw resistance of steel fibre*
750 *reinforced rubberised concrete*, Construction and Building Materials 195 (2019) 450-458.
- 751 [31] V. Baroghel-Bouny. *Evaluation and prediction of reinforced concrete durability by means of*
752 *durability indicators. Part I: new performance-based approach. in ConcreteLife'06-*
753 *International RILEM-JCI Seminar on Concrete Durability and Service Life Planning: Curing,*
754 *Crack Control, Performance in Harsh Environments. 2006: RILEM Publications SARL.*
- 755 [32] M. Alexander, J. Mackechnie, and Y. Ballim, *Guide to the use of durability indexes for achieving*
756 *durability in concrete structures*, Research monograph 2 (1999).
- 757 [33] Swedish standards, *SS 13 72 44 ED. 4. Concrete Testing - Hardened Concrete - Scaling At*
758 *Freezing. Standardiserings-Kommissionen I Sverige*, (2005).
- 759 [34] RILEM, *TC 176-IDC: Internal damage of concrete due to frost action, Final Recommendation,*
760 *Prepared by L. Tang and P.-E. Petersson SP Swedish National Testing and Research Institute,*
761 *Boras, Sweden. Materials and Structures / Matériaux et Constructions, Vol. 37, December*
762 *2004, pp 754-759 in Slab test: Freeze/thaw resistance of concreteInternal deterioration 2004.*
- 763 [35] ETRA, *The European Tyre Recycling Association. 2016, Available at: <http://www.etra-eu.org>*
764 *[Last accessed: 02/01/2018].*
- 765 [36] S. Goel, S. Singh, and P. Singh, *Fatigue analysis of plain and fiber-reinforced self-consolidating*
766 *concrete*, Materials Journal 109 (5) (2012) 573-582.
- 767 [37] B.H. Oh, *Fatigue analysis of plain concrete in flexure*, Journal of structural engineering 112 (2)
768 (1986) 273-288.
- 769 [38] H. Hu, P. Papastergiou, H. Angelakopoulos, M. Guadagnini, and K. Pilakoutas, *Mechanical*
770 *properties of SFRC using blended manufactured and recycled tyre steel fibres*, Construction
771 and Building Materials 163 (2018) 376-389.
- 772 [39] ASTM, *C136: Standard test method for sieve analysis of fine and coarse aggregates. ASTM*
773 *International, West Conshohocken, PA. doi:10.1520/C0136-06. 2006.*
- 774 [40] BSI, *EN 12390-2: Testing hardened concrete, Part 2: Making and curing specimens for strength*
775 *tests. BSI 389 Chiswick High Road, London W4 4AL, UK. 2009.*

- 776 [41] BSI, *EN 12390-3: Testing hardened concrete, Part3: Compressive strength of test specimens*.
777 *BSI 389 Chiswick High Road, London W4 4AL, UK*. 2009.
- 778 [42] JSCE, *SF-4: Method of test for flexural strength and flexural toughness of steel fiber reinforced*
779 *concrete*. Japan Concrete Institute, Tokio, Japan., (1984).
- 780 [43] S. Singh and S. Kaushik, *Flexural fatigue life distributions and failure probability of steel fibrous*
781 *concrete*, Materials Journal 97 (6) (2000) 658-667.
- 782 [44] S. Singh, B. Ambedkar, Y. Mohammadi, and S. Kaushik, *Flexural fatigue strength prediction of*
783 *steel fibre reinforced concrete beams*, Electronic Journal of Structural Engineering 8 (1) (2008)
784 46-54.
- 785 [45] RILEM, *TC 162-TDF: Test and design methods for steel fibre reinforced concrete, Bending test,*
786 *Final Recommendation. Materials and Structures: 35, 579-582*. 2002.
- 787 [46] B. Zhang, D. Phillips, and K. Wu, *Effects of loading frequency and stress reversal on fatigue life*
788 *of plain concrete*, Magazine of Concrete Research 48 (177) (1996) 361-375.
- 789 [47] M. Darter and E. Barenberg, *DESIGN OF ZERO MAINTENANCE PLAIN JOINTED CONCRETE*
790 *PAVEMENT, VOLUME TWO-DESIGN MANUAL*. 1977.
- 791 [48] J.R. Roesler, *Fatigue of concrete beams and slabs*. 1998.
- 792 [49] S. Singh and S. Kaushik, *Fatigue strength of steel fibre reinforced concrete in flexure*, Cement
793 and Concrete Composites 25 (7) (2003) 779-786.
- 794 [50] B.H. Oh, *Fatigue life distributions of concrete for various stress levels*, Materials Journal 88 (2)
795 (1991) 122-128.
- 796 [51] Y. Mohammadi and S. Kaushik, *Flexural fatigue-life distributions of plain and fibrous concrete*
797 *at various stress levels*, Journal Of Materials In Civil Engineering 17 (6) (2005) 650-658.
- 798 [52] S. Singh, B. Singh, and S. Kaushik, *Probability of fatigue failure of steel fibrous concrete*,
799 Magazine of Concrete Research 57 (2) (2005) 65-72.
- 800 [53] J.T. McCall. *Probability of fatigue failure of plain concrete*. in *Journal Proceedings*. 1958.
- 801 [54] H. Westergaard, *Stresses in concrete pavements computed by theoretical analysis*, Public
802 roads (1926).
- 803 [55] G. Garber, *Design and construction of concrete floors*. 2006: CRC Press.
- 804 [56] TR34, *The Concrete Society: Concrete industrial ground floors – a guide to design and*
805 *construction*. 4rd ed. Technical Report 34; 2013.
- 806 [57] Abaqus, *6.14 Abaqus Theory Manual*. USA:Dassault Systemes Simulia Corporation, 651
807 (2014).
- 808 [58] J. Hua, *Finite element modeling and analysis of accelerated pavement testing devices and*
809 *rutting phenomenon*, (2000).
- 810 [59] I. ARA, ERES Consultants Division., *Guide for Mechanistic–Empirical Design of New and*
811 *Rehabilitated Pavement Structures*, Final Rep., NCHRP Project 1-37A (2004).
- 812 [60] H. Jiang and Y. Xie, *A note on the Mohr–Coulomb and Drucker–Prager strength criteria*,
813 Mechanics Research Communications 38 (4) (2011) 309-314.
- 814 [61] N. Jafarifar, K. Pilakoutas, H. Angelakopoulos, and T. Bennett, *Post-cracking tensile behaviour*
815 *of steel-fibre-reinforced roller-compacted-concrete for FE modelling and design purposes*,
816 (2017).
- 817 [62] P. Casanova and P. Rossi, *Analysis and design of steel fiber reinforced concrete beams*,
818 Structural Journal 94 (5) (1997) 595-602.
- 819 [63] N. Jafarifar, K. Pilakoutas, and T. Bennett, *Moisture transport and drying shrinkage properties*
820 *of steel–fibre-reinforced-concrete*, Construction and Building Materials 73 (2014) 41-50.
- 821 [64] B. Mobasher, *Mechanics of fiber and textile reinforced cement composites*. 2011: CRC press.
- 822
- 823